



Published in final edited form as:

Nat Chem. 2010 January 31; 2: 179–186. doi:10.1038/nchem.545.

Watching conformational- and photo-dynamics of single fluorescent proteins in solution

Randall H. Goldsmith and W. E. Moerner

Department of Chemistry, Stanford University, Stanford, CA 94305

Abstract

Observing the dynamics of single biomolecules over prolonged time periods is difficult to achieve without significantly altering the molecule through immobilization. It can, however, be accomplished using the Anti-Brownian ELectrokinetic (ABEL) Trap, which allows extended investigation of solution-phase biomolecules - without immobilization - through real-time electrokinetic feedback. Here we apply the ABEL trap to study an important photosynthetic antenna protein, Allophycocyanin (APC). The technique allows the observation of single molecules of solution-phase APC for more than one second. We observe a complex relationship between fluorescence intensity and lifetime that cannot be explained by simple static kinetic models. Light-induced conformational changes are shown to occur and evidence is obtained for fluctuations in the spontaneous emission lifetime, which is typically assumed to be constant. Our methods provide a new window into the dynamics of fluorescent proteins and the observations are relevant for the interpretation of in vivo single-molecule imaging experiments, bacterial photosynthetic regulation, and biomaterials for solar energy harvesting.

The investigation of single biomolecules allows the observation of unsynchronized or rare events that are impossible to observe in ensemble measurements.^{1–6} Solution-phase single-molecule spectroscopy^{6–8} is particularly challenging as one must balance the desire to make measurements for the prolonged periods of time required for detection of a statistically robust numbers of photons over multiple timescales, with the experimental reality that techniques for biomolecule immobilization may alter the molecular dynamics or contribute to the same inhomogeneous broadening that one hopes to eliminate by doing a single-molecule measurement.⁹ In some cases, rigorous efforts show the persistence of native structure after surface immobilization through comparison with bulk assays¹⁰ or confinement in vesicles.¹¹ However, in other cases doubts remain as to how immobilization affects more subtle facets of biomolecule behavior, such as conformational dynamics.^{12, 13}

Users may view, print, copy, download and text and data- mine the content in such documents, for the purposes of academic research, subject always to the full Conditions of use: http://www.nature.com/authors/editorial_policies/license.html#terms

Correspondence to: W. E. Moerner.

Author contributions

R.H.G. and W.E.M. conceived and designed the experiments; R.H.G. performed the experiments; R.H.G. and W.E.M analyzed the data, and co-wrote the paper.

Additional information

Supplementary information accompanies this paper at www.nature.com/naturechemistry. Reprints and permission information is available online at <http://npg.nature.com/reprintsandpermissions/>.

In this work we employ the Anti-Brownian ELectrokinetic (ABEL) trap^{14, 15} to examine the photophysics of a single fluorescent protein, Allophycocyanin (APC), *in solution*. The ABEL trap maintains the position of the fluorescent protein at the center of a microfluidic cavity, where it can be probed for prolonged periods of time (often >1 s) without immobilization. The ABEL trap provides some advantages of surface immobilization (long observation time) and open-volume detection (minimal surface interaction) without their disadvantages (structural perturbation; short observation time and significant spatial excitation intensity variation). By directly measuring time-dependent changes in APC's fluorescence intensity and lifetime, we obtain an unprecedented view into the dynamics of a single fluorescent protein in solution. Changes in chromophore photophysics offer a means to probe protein conformational dynamics in real time.³ We observe a complex relationship between fluorescence intensity and lifetime that is poorly described by the common assumption of a static radiative rate. This behavior suggests light-induced conformational dynamics may be important for quantitative treatment of Forster Resonance Energy Transfer (FRET) involving fluorescent proteins that forms the basis for certain *in vivo* single-molecule¹⁶ and fluorescence lifetime imaging microscopy (FLIM) investigations.¹⁷ Additionally, novel intensity-lifetime dynamics can have implications for understanding bacterial photoprotection mechanisms and the use of biomaterials in solar energy applications.

The ABEL trap controls the position of a fluorescent object by using two orthogonal pairs of electrodes to drive electroosmotic flows that cancel the object's Brownian motion within a microfluidic environment.^{14, 15} The biomolecule's position is estimated using a rapidly rotating laser spot and lock-in detection;^{15, 18, 19} the correct force vector to return the molecule to the center of the trap is calculated with a homebuilt analog circuit phase-locked to the rotating spot, which uses the actual time of photon detection to estimate the position of the molecule. This technique allows trapping of objects significantly smaller than those that can be stably trapped by optical tweezers, including single chromophores.¹⁵ Recently, single strands of fluorescently labeled DNA were trapped in the ABEL trap, allowing visualization and analysis of chain dynamics that would be unobservable in bulk measurements and substantially altered by immobilization.²⁰

The target for this study, APC, is a photosynthetic antenna protein found in red algae and cyanobacteria where it is an important component of the phycobilisome, a protein-superstructure exciton funnel that directs energy toward the photosynthetic reaction center.²¹ It is a disc-like trimer ($\alpha\beta$)₃, 11 nm in diameter and 3 nm thick, with each monomer ($\alpha\beta$) comprised of strongly bound α and β subunits.²² Photophysical properties of APC are dominated by six covalently-bound phycocyanobilin (PCB) molecular cofactors that form three pairs at the interfaces between the protein monomers upon fulfillment of the protein's native quaternary structure, Fig 1.²¹ The center-center distance between paired chromophores is 2.1 nm.²² A strong excitonic interaction within these pairs was conclusively demonstrated via ultrafast transient anisotropy.²³ After rapid electronic dephasing and localization,²⁴ excitons may hop between PCB's of the same or different pairs via FRET.^{22, 25} Two reports have examined APC at the single-molecule level, with one group²⁶ immobilizing APC in polyvinyl alcohol (PVA) and the other²⁷ using agarose or

non-specific adsorption on glass. Interestingly, these studies show different photobleaching behavior of APC, with one group observing up to six distinct photobleaching steps²⁶ and the other up to three.²⁷ Consequently, APC seems particularly well-suited for solution-phase investigation without immobilization.

Results

Multiple Intensity Levels

Single molecules of APC, upon diffusion into the excitation volume, are localized at the center of the trap and experience spatially flat excitation from the rapidly rotating laser spot. Once in the trap, intensity changes, Fig. 2, are primarily from molecular photo-dynamics, unlike fluorescence correlation spectroscopy (FCS) where diffusion in a nonuniform Gaussian spot introduces additional intensity fluctuations. Multiple stepped intensity levels have previously been observed in immobilized APC^{26, 27} and are a common feature of weakly-coupled multi-chromophore systems.^{4, 5} To count the number of intensity levels per APC, we employed the change-point-finding algorithm of Watkins and Yang²⁸ which yields the blue traces in Fig. 2 and faithfully captures the stepped intensity behavior.

As seen in Fig. 2, similar intensity levels are often visited multiple times. To evaluate the number of *distinct* levels per burst we combine the agglomerative hierarchical grouping method of Watkins and Yang²⁸ with evaluation via the Bayesian Information Criterion (BIC). A histogram of the number of distinct levels identified from each APC molecule is shown in Fig. 3a and suggests at least four distinct intensity levels. At least four distinct levels is obvious from Fig. 2 as well. This number parallels that for APC immobilized in PVA²⁶ but contrasts with APC immobilized in agarose or on glass where a maximum of three levels was observed²⁷ and suggests that some immobilization environments may cause APC to deviate from its solution-phase behavior.

Fluorescence Lifetime Fluctuations

Time-stamping of recorded photons relative to each excitation pulse opens a second channel for observing the dynamics of solution-phase fluorescent proteins.⁶ Histogramming arrival times from photons collected over a given time interval allows visualization of the fluorescence decay, Fig. 3c,d. The intensity change-points determined above define intervals for pooling arrival times. The ABEL trap frequently enables the recording of many thousands of photons from each molecule allowing robust analysis, an improvement over open-volume methods without feedback where over one order of magnitude less photons are typically collected.

Most intervals show a relatively constant fluorescence lifetime, as verified by subdividing the interval and refitting the decays. After assigning lifetimes to each intensity interval, we histogram the number of photons detected with various fluorescence lifetimes, Fig 3b. This highly asymmetric distribution requires at least three Gaussians for an adequate fit. The highest peak has a full width at half maximum (FWHM) of 0.13 ns. This is significantly smaller than the FWHM of approximately 0.55 ns for the analogous peak in molecules of APC trapped in PVA.²⁶ This reduction implies that immobilization has a tangible effect on

the photo-dynamics of APC and contributes to inhomogeneous broadening of APC's lifetime. Importantly, these effects are much reduced in our solution-phase experiment. A more detailed comparison is found in the Supplementary Information.

In Fig. 2, calculated fluorescence lifetimes are plotted alongside intensity fluctuations. It is evident that while these two channels are usually correlated, they are sometimes uncorrelated or anti-correlated. A diversity of behavior was also seen in immobilized APC.^{26, 27} To investigate, we plotted for each intensity interval, the average intensity vs. the determined fluorescence lifetime, Fig. 4a, for 1,048 individual APC molecules. Each marker indicates one point in the intensity-lifetime trajectory of one APC molecule. The intensity-lifetime trajectory of the APC molecule in Figure 2d is shown in red in Fig. 4a, with eight intensity plateaus represented by eight data points. Two salient features are evident. First, a high concentration of data points occurs near 20 cps and 1.5 ns, Fig. 4b. Second, there is a smooth continuum of intensity-lifetime values with lower intensities generally correlating with lower and more widely distributed lifetimes. While fewer photons are generally recorded for lower intensity intervals, enough are obtained to have good statistical confidence with most data points having expected standard deviations < 0.1 ns, Fig. S2. To visualize the transitions, each individual jump in the intensity-lifetime trajectory is plotted as a vector starting at the origin in Fig. 4c. Most shifts to lower intensities are accompanied by shifts to lower lifetimes (quadrants 1,3). This relationship between fluorescence intensity and lifetime is expected for weakly-coupled multi-chromophoric systems since the dark states that result in incremental loss of fluorescence intensity may also partially quench remaining active emitters, leading to a shorter lifetime. Unexpectedly, a statistically robust minority (13%) show the reverse correlation.

Surprisingly, ~ 1 – 2% of intensity intervals show significant lifetime fluctuations at near constant intensity as determined by successive binning of every 500 photons and displayed in the green trace in Fig. 5a,b. Fluorescence decays and fits for high and low lifetime regions in the same intensity interval are shown in Figs. S3–S7 and have conspicuously different time constants. Fluctuations in lifetime at constant intensity^{29, 30} are very unusual due to the algebraic relationship between lifetime and quantum yield³¹ and will be further discussed below. Large shifts (> 4 standard deviations) in lifetime at near constant intensity are also recorded in Fig 4c along the y-axis.

Discussion

Microstate properties and transitions

Essential to understanding the solution-phase dynamics of APC is the number of underlying microstates for one molecule during its time in the trap. Several methods exist for discerning the number of microstates in single-molecule systems, including Expectation-Maximization clustering²⁸ and Hidden Markov Models (HMM).³² For APC we desire a method that preserves the divisions found above by the change-point-finding algorithm,²⁸ since these intervals successfully capture much of the intensity dynamics, and a method that includes the time-ordering of the data, since each lifetime-intensity data point in Fig. 4a is one point in a single APC's trajectory (red trace). We developed a Time-Order Clustering (TOC) method that is further described in the Methods section and Supplementary Information.

TOC seeks to explain the state changes with the smallest number of parameters using statistical methods to choose between alternatives and suggests four contributing states with properties summarized in Fig 6a-c.

Figure 6d offers a succinct description of state dynamics and includes inter-state rate constants calculated from TOC. Upon entering the ABEL trap, most “fresh” APC molecules (67%) belong to State 1, with a high intensity and narrow lifetime distribution. This fraction is likely underestimated, as previously probed molecules frequently reentered the trap during experiments performed at substantially lower concentration. The molecule then has comparable rates of shifting into States 2 and 3. While return to more fluorescent states is possible, most state shifts (68%) are to dimmer states where the molecule becomes increasingly likely to completely photobleach or be lost by the trap. Though strong coupling initially exists between the two PCB’s of each of APC’s three chromophore pairs, the observation of at least four emissive states suggests that each state cannot be simply correlated to each chromophore pair successively becoming dark. This observation, combined with blue shifting of the emission maxima sometimes accompanying decrease in fluorescence intensity,²⁶ and more than three states being observed in polarization anisotropy measurements,²⁶ led Loos et al. to conclude that decreases in fluorescence intensity can stem from only a single member of the pair becoming dark, leading to up to six fluorescence intensity levels.²⁶ Our results support this picture in solution-phase APC. Observation of only four states is consistent with Fig. 3a and likely a result of APC molecules in minimally luminous states being difficult to confine in the ABEL trap.

Dynamic conformational diversity

Within the four primary states (Fig. 6), the continuous distribution of intensities and lifetimes rather than discrete groupings strongly suggests conformational diversity among APC molecules. This explanation is supported by the inherent sensitivity of the fluorescence quantum yield (Φ) of PCB to its protein environment,³³ with conformational changes in biliproteins initiated by a denaturant appearing as changes in Φ before changes were observed in absorption spectra or circular dichroism.^{33, 34} The protein’s conformation is integral to APC being a bright emitter, with bulk APC in buffer demonstrating an excellent quantum yield with $\Phi=0.68$ and fluorescence lifetime $\tau=1.6$ ns (majority component).²⁶ Bare PCB in solution is nearly completely quenched with $\tau<40$ ps³⁵ due to a complex combination of Z→E isomerization about exocyclic olefins, internal conversion owing to PCB’s flexibility, and excited state proton transfer, with relative magnitudes of each component depending on PCB’s instantaneous geometry.³⁶ APC maintains a high Φ by keeping PCB “stretched-out” on a protein scaffold via covalent and non-covalent interactions, Fig 1.²² A broad distribution of PCB conformers as a result of subtle changes to protein conformation is likely the primary contributor to the observed continuum of intensities and lifetimes.

However, this lifetime diversity is absent in the tight grouping at 20 cpms, Fig. 4a,b, that comprises the majority of State 1, Fig. 6c. As described above, most APC molecules entering the ABEL trap belong to State 1 and show this narrow lifetime distribution. In addition, the fluorescence decay in bulk samples is multi-exponential with 90% of the

fluorescence decay amplitude coming from a 1.6 ns component (with the rest from a faster component).²⁶ These two observations suggest the majority of APC molecules exist in State 1, their native state, before photoexcitation. A relatively homogenous population of APC molecules enters the ABEL trap, but upon prolonged excitation, molecules shift to dimmer states with larger lifetime distributions, Fig. 6, implying not only static diversity but dynamic diversity as well.

Large-scale intensity jumps between states likely result from formation of non-emissive radical cations, which have been directly observed upon UV excitation³⁷ while charged photocarriers have been observed upon visible excitation in photovoltaic studies.³⁸ Coulombic interactions between PCB-centered cations and the protein matrix likely cause conformational changes. Electron transfer reactions have been shown to electrostatically cause significant internal motions in proteins with embedded redox centers like the photosynthetic reaction center³⁹ and to cause local unfolding as a result of even non-specifically bound sensitizers for photo-induced electron transfer.⁴⁰

Photophysical consequences of conformational changes

Protein conformational diversity can explain the range of observed photophysical trajectories in Fig. 4a,c. Decreases in intensity are expected to be accompanied by decreases in lifetime (Fig. 4c, quadrants 1,3) as cations, acting as energy sinks, should effectively quench distal emitters via FRET²⁶ due to favorable spectral overlap³⁷ and rapid non-radiative decay. This relationship is supported by a correlation between the size of the intensity drop between consecutive intervals and the lifetime of the product state: large transitions from State 1 to State 4 result in a member of State 4 with a mean τ of 0.55 ns, whereas the mean τ values for smaller transitions from States 3 or 2 to State 4 are 0.72 and 0.90 ns, respectively. This correlation makes sense, as a small drop in fluorescence intensity can arise from a non-quenching dark state since it will leave non-perturbed chromophores fully emissive, while larger decreases in fluorescence intensity require affecting multiple chromophores simultaneously through a long-distance interaction like FRET and will consequently display a shorter lifetime, as observed.

Fluorescence intensity changes at near constant lifetime (Fig. 4c, x-axis) are indicative of a non-quenching dark state. Cation formation can lead to reductions in intensity, but with small or negligible changes in lifetime if the conformation of the chromophore bearing the cation has shifted to display poor spectral overlap or orientation to quench its neighbors. The range of slopes near the x-axis supports this picture. The extinction coefficient of PCB is also a function of conformation,⁴¹ although this change is also expected to affect lifetime. Additionally, conformational changes may alter the extinction coefficient by affecting the degree of exciton coupling within a PCB dimer.

More exotic behavior is seen in quadrant 2, Fig. 4c, where an unexpected increase in lifetime accompanies decreasing intensity. 82% of molecules exhibiting a quadrant 2 transition have previously visited states 2, 3, or 4 implying the prior formation of cations and consequent local denaturation. Trajectories along the y-axis of Fig. 4c, displayed in Fig. 5a,b, are also unexpected as changes in lifetime at constant intensity are very rare. Such changes were seen in highly fluorescent ($\Phi \sim 1$) dyes embedded in a polystyrene matrix by

Vallée,²⁹ who inferred a fluctuating spontaneous (natural) emission lifetime, τ_{RAD} . This possibility is appealing here due to the relationship between the average intensity (AI), quantum yield (Φ) and the rate equations relating Φ , τ , τ_{RAD} , and the characteristic time of non-radiative processes, τ_{Q} ,³¹ wherein Φ is far more sensitive to changes in τ_{Q} than τ_{RAD} .⁴

$$AI(\text{cpms}) \propto \Phi = \frac{\tau_{\text{RAD}}^{-1}}{\tau_{\text{RAD}}^{-1} + \tau_{\text{Q}}^{-1}} = \frac{\tau_{\text{RAD}}^{-1}}{\tau^{-1}}$$

In Fig. 5b, the trapped APC shifts from a lifetime of 0.81 to 1.27 ns with negligible change in fluorescence intensity. Assuming a constant τ_{RAD} that can be calculated from bulk measurements of Φ and τ , and that only τ_{Q} is changing (the usual assumptions), the intensity should jump from the observed value of 7 to >11 cpms, which is clearly not observed. In contrast, assuming a constant τ_{Q} and variable τ_{RAD} predicts a shift from 7 to 6 cpms, a much smaller change. Figure 5c shows two curves of constant observed lifetime, τ , corresponding to the starred intervals in Fig. 5b. Transitions from $\tau=0.81 \rightarrow 1.27$ with constant τ_{RAD} require an increase in Φ . Transitions with constant τ_{Q} , however, require a decrease in Φ and can explain transitions in Fig. 4c, quadrants 2,4. Transitions at near constant Φ , as in Fig. 5b, require changes in τ_{RAD} and τ_{Q} . Simultaneous changes in τ_{Q} and τ_{RAD} would result in a diversity of correlations between lifetime and intensity, as observed experimentally, Fig. 4c. Observation of this diversity provides strong evidence of a fluctuating τ_{RAD} .

The origin of variations in τ_{RAD} described by Vallée²⁹ lies in changes in the microscopic environment of each chromophore. Specifically in this model, chromophores experience a fluctuating polarizable polymer solvation shell where introduction of voids results in a shifting dielectric profile and consequently shifting τ_{RAD} .³⁰ A similar situation exists in a biological setting where partial denaturation in the vicinity of the chromophore could also result in a shifting dielectric environment and consequent shifting of τ_{RAD} . A dynamic τ_{RAD} was previously suggested in light-harvesting complexes⁴, bilirubin-albumin complexes,⁴² and chromophores embedded in membrane rafts,⁴³ with the latter study employing an adapted version of Vallée's model. In APC multiple charged or aromatic residues are proximal to PCB²² and changes in their formal charge or orientation will influence the dielectric environment. PCB's are positioned close to the protein-solvent interface, Fig. 4d, and varying infiltration of solvent into the chromophore's micro-environment can also play a role due to dielectric contrast between the solvent and the protein's interior.⁴⁴ Finally, changes in the conformation and polarizability of PCB itself will affect τ_{RAD} and will provide an interesting target system for molecular dynamics simulations.

Conclusion

By allowing a new way of probing solution-phase protein dynamics, the ABEL trap revealed previously hidden photo-dynamics at the single-molecule level, including light-induced conformational changes. Evidence of modulation of the spontaneous emission lifetime, which is usually assumed constant, was observed and is likely linked to these conformational changes. Similar conformational and photo-dynamics are likely present in

other fluorescent proteins such as Green Fluorescent Protein (GFP) and will be particularly conspicuous in other multi-chromophoric proteins. These dynamics have implications for the widespread use of lifetimes measured from fluorescent proteins in bio-imaging where changing lifetimes are frequently attributed uniquely to the changing population or orientation of an external quencher. Additionally, photo-induced denaturation appears to be another form of photodamage that can occur under intense illumination and highlights the need for cellular protection mechanisms. Finally, this photodamage must be addressed for strongly pumped chromophores in proteins to be used for solar energy applications.

Methods

Sample Preparation

ABEL trap cells made of fused silica with 700 nm cell depth were constructed as previously described.¹⁵ Cell interiors were coated with two pairs of layers of polyethylene imine (PEI) and polyacrylic acid (PAA) ending in PAA to prevent non-specific adsorption.⁴⁵ Without this treatment, we observed conspicuous sticking of APC to the surfaces of the trap. Covalently cross-linked APC⁴⁶ was purchased from Molecular Probes as in the other single-molecule studies^{26, 27} and purified as instructed. APC was diluted in a 1:1 (v/v) mixture of 0.1 M PBS buffer at pH=7.5 and glycerol. APC has been shown to be minimally perturbed in this solvent mixture.⁴⁷ Sample solutions were diluted to a final concentration of 0.06 nM immediately before data collection with a glycerol:buffer mixture that had been sparged with Argon for at least 25 minutes. All experiments were performed under a blanket of Argon due to APC's production of several reactive oxygen species upon excitation in air and significantly higher photostability under inert atmosphere.⁴⁸

Excitation, Detection, and Feedback

Excitation was provided by the spectrally filtered supercontinuum output of a non-linear photonic crystal fiber (Femto White 800, Newport) pumped by a mode-locked Ti:Sapphire laser (790 nm, 200 fs pulse length, 76 MHz repetition rate, Mira 900, Coherent) yielding pulses centered at 596 nm with FWHM of 3 nm and length < 3 ps. The laser light was steered into the epi-port of a Nikon TE-3000 microscope and focused with an oil objective (NA=1.0) to provide an average power of 1.7 kW/cm² at the sample. Beam deflection to produce the rotating spot is achieved through the same apparatus described previously.¹⁵ The excitation spot is 0.8 μ m in diameter in the sample plane, as measured by scanning a fluorescent bead through the focal volume, and is rotated at 40 KHz with a radius of 0.33 μ m in the sample plane. Sample fluorescence is collected back through the same objective and passed through dichroic (620DCLP) and long pass (HQ620LP) filters, a 200 μ m pinhole and focused onto an APD (Perkin Elmer, SPCM-OD 2801). Time-correlated single-photon counting (TCSPC) is achieved using the PicoHarp 300 (Picoquant) timing module. A total instrument response function (IRF) of 0.3 ns was measured from scatter from a glass coverslip. Feedback direction and magnitude are calculated for each 25 μ s cycle by phase-sensitive integration of photons detected in the previous cycle. A single detected photon produces a feedback pulse of 24 V vector magnitude lasting 25 μ s which is applied across the 20 μ m transverse width of the shallow region of the cell.¹⁵ This field is expected to have a negligible effect on the absorption spectra, as described in the Supplementary Information.

Voltages are produced by four PA-83 high voltage operational amplifiers (Apex Microtechnologies) to generate forces in the appropriate direction to cancel Brownian motion.

Experiments were also repeated with a CW 638 nm excitation source (FiberTEC, Blue Sky) and showed qualitatively similar results, albeit with longer survival times, as observed previously.²⁷ A fraction of fluorescence bursts showed short lived intensity spikes between 25–50 cps. The fraction showing this level decreased as a function of sample concentration and was assumed to originate from two APC molecules briefly co-occupying the trap. Simulations confirmed this explanation and these bursts were eliminated from all analysis.

Data Analysis

All calculations were implemented in Matlab. The change-point-finding algorithm²⁸ was applied to 1 ms binned data. Modeling the fluorescence decays is accomplished via the method of Zander.⁴⁹ Standard deviations in parameter determination are calculated from the observed Fisher information.⁵⁰ Error bars in Fig. 5a,b represent ± 1 standard deviation. More detailed calculations are given in the Supplementary Information.

In the agglomerative clustering analysis,²⁸ a maximum or leveling off of the BIC indicates proper dimensionality has been identified. The number of APC molecules exhibiting higher numbers of levels (>4) is dependent on the threshold used to identify the leveling off of the BIC. However, the existence of at least four distinct intensity levels is independent of this threshold.

Time-Order Clustering (TOC) classifies states based on their proximity to a center intensity value (similar to k-means) with a conditional reclassification procedure for consecutive intervals. Classifications are judged with a HMM analysis in the evaluation configuration, where the likelihood of observing the experimental data (x_k) is determined given the inferred descriptions of the microstates, including intensity center value (Ic_i) and variance ($I\sigma_i$), and transition probabilities ($t_{i \rightarrow j}$) between states, which can be determined from the TOC state assignments.

$$L = HMM_E(x_k, Ic_i, I\sigma_i, t_{i \rightarrow j})$$

Leveling off of the likelihood (Fig. S8) suggests four contributing states, with assignments and properties shown in Fig. 6. A more detailed description is given in the Supplementary Information. Transition probabilities can be used to calculate inter-state rate constants by the relationship

$$k_{i \rightarrow j} = -\ln(1 - t_{i \rightarrow j})$$

Rate constants used to create Fig. 6d and transition matrix probabilities are shown in Tables S1 and S2.

Supplementary Material

Refer to Web version on PubMed Central for supplementary material.

Acknowledgments

We gratefully acknowledge support from Yan Jiang; we thank Alex Fürstenberg, Quan Wang, Sam Bockenbauer, Michael Thompson, and Lana Lau for helpful discussions and Adam Cohen for initial trap design and quartz lithography. This work was supported in part by the U. S. Department of Energy Grant No. DE-FG02-07ER15892 and by Grant No. 1R21-RR023149 from the National Center for Research Resources of the National Institutes of Health.

References

1. Moerner WE, Orrit M. Illuminating Single Molecules in Condensed Matter. *Science*. 1999; 283:1670–1676. [PubMed: 10073924]
2. Myong S, et al. Cytosolic Viral Sensor RIG-I Is a 5'-Triphosphate-Dependent Translocase on Double-Stranded RNA. *Science*. 2009; 323:1070–1074. [PubMed: 19119185]
3. Hofmann C, Aartsma TJ, Michel H, Kohler J. Direct observation of tiers in the energy landscape of a chromoprotein: A single-molecule study. *Proc Natl Acad Sci USA*. 2003; 100:15534–15538. [PubMed: 14671325]
4. Bopp MA, Jia Y, Li L, Cogdell RJ, Hochstrasser RM. Fluorescence and photobleaching dynamics of single light-harvesting complexes. *Proc Natl Acad Sci USA*. 1997; 94:10630–10635. [PubMed: 9380686]
5. Hofkens J, et al. Probing photophysical processes in individual multichromophoric dendrimers by single-molecule spectroscopy. *J Am Chem Soc*. 2000; 122:9278–9288.
6. Rothwell PJ, et al. Multiparameter single-molecule fluorescence spectroscopy reveals heterogeneity of HIV-1 reverse transcriptase:primer/template complexes. *Proc Natl Acad Sci USA*. 2003; 100:1655–1660. [PubMed: 12578980]
7. Nie S, Chiu DT, Zare RN. Probing individual molecules with confocal fluorescence microscopy. *Science*. 1994; 266:1018–1021. [PubMed: 7973650]
8. Shera EB, Seitzinger NK, Davis LM, Keller RA, Soper SA. Detection of Single Fluorescent Molecules. *Chem Phys Lett*. 1990; 174:553–557.
9. Rasnik I, McKinney SA, Ha T. Surfaces and Orientations: Much to FRET About? *Acc Chem Res*. 2005; 38:542–548. [PubMed: 16028888]
10. Rasnik I, Myong S, Cheng W, Lohman TM, Ha T. DNA-binding orientation and domain conformation of the E-coli Rep helicase monomer bound to a partial duplex junction: Single-molecule studies of fluorescently labeled enzymes. *J Mol Biol*. 2004; 336:395–408. [PubMed: 14757053]
11. Okumus B, Wilson TJ, Lilley DMJ, Ha T. Vesicle encapsulation studies reveal that single molecule ribozyme heterogeneities are intrinsic. *Biophys J*. 2004; 87:2798–2806. [PubMed: 15454471]
12. Friedel M, Baumketner A, Shea JE. Effects of surface tethering on protein folding mechanisms. *Proc Natl Acad Sci USA*. 2006; 103:8396–8401. [PubMed: 16709672]
13. Talaga DS, et al. Dynamics and folding of single two-stranded coiled-coil peptides studied by fluorescent energy transfer confocal microscopy. *Proc Natl Acad Sci USA*. 2000; 97:13021–13026. [PubMed: 11087856]
14. Cohen AE, Moerner WE. Suppressing Brownian motion of individual biomolecules in solution. *Proc Natl Acad Sci USA*. 2006; 103:4362–4365. [PubMed: 16537418]
15. Cohen AE, Moerner WE. Controlling Brownian motion of single protein molecules and single fluorophores in aqueous buffer. *Opt Express*. 2008; 16:6941–6956. [PubMed: 18545398]
16. Murakoshi H, et al. Single-molecule imaging analysis of Ras activation in living cells. *Proc Natl Acad Sci U S A*. 2004; 101:7317–7322. [PubMed: 15123831]

17. Lee SJR, Escobedo-Lozoya Y, Szatmari EM, Yasuda R. Activation of CaMKII in single dendritic spines during long-term potentiation. *Nature*. 2009; 458:299–304. [PubMed: 19295602]
18. Berglund AJ, Mabuchi H. Feedback controller design for tracking a single fluorescent molecule. *Appl Phys B*. 2004; 78:653–659.
19. Enderlein J. Tracking of fluorescent molecules diffusing within membranes. *Appl Phys B*. 2000; 71:773–777.
20. Cohen AE, Moerner WE. Principal-components analysis of shape fluctuations of single DNA molecules. *Proc Natl Acad Sci USA*. 2007; 104:12622–12627. [PubMed: 17496147]
21. MacColl R. Allophycocyanin and energy transfer. *Biochim et Biophys Acta*. 2004; 1657:73–81.
22. Brejc K, Ficner R, Huber R, Steinbacher S. Isolation, crystallization, crystal structure analysis and refinement of allophycocyanin from the cyanobacterium *Spirulina platensis* at 2.3 Å resolution. *J Mol Biol*. 1995; 249:424–440. [PubMed: 7783202]
23. Edington MD, Riter RE, Beck WF. Evidence for Coherent Energy-Transfer in Allophycocyanin Trimers. *J Phys Chem*. 1995; 99:15699–15704.
24. Edington MD, Riter RE, Beck WF. Interexciton-state relaxation and exciton localization in allophycocyanin trimers. *J Phys Chem*. 1996; 100:14206–14217.
25. Beck WF, Sauer K. Energy-Transfer and Exciton-State Relaxation Processes in Allophycocyanin. *J Phys Chem*. 1992; 96:4658–4666.
26. Loos D, Cotlet M, De Schryver FC, Habuchi S, Hofkens J. Single-Molecule Spectroscopy Selectively Probes Donor and Acceptor Chromophores in the Phycobiliprotein Allophycocyanin. *Biophys J*. 2004; 87:2598–2608. [PubMed: 15454454]
27. Ying L, Xie XS. Fluorescence Spectroscopy, Exciton Dynamics, and Photochemistry of Single Allophycocyanin Trimers. *J Phys Chem B*. 1998; 102:10399–10409.
28. Watkins LP, Yang H. Detection of Intensity Change Points in Time-Resolved Single-Molecule Measurements. *J Phys Chem B*. 2005; 109:617–628. [PubMed: 16851054]
29. Vallee RAL, et al. Fluorescence lifetime fluctuations of single molecules probe the local environment of oligomers around the glass transition temperature. *J Chem Phys*. 2007; 126
30. Vallee RAL, Van Der Auweraer M, De Schryver FC, Beljonne D, Orrit M. A microscopic model for the fluctuations of local field and spontaneous emission of single molecules in disordered media. *Chem Phys Chem*. 2005; 6:81–91. [PubMed: 15688651]
31. Lakowicz, JR. Principles of fluorescence spectroscopy. Vol. 954. Springer Science; New York: 2006.
32. McKinney SA, Joo C, Ha T. Analysis of single-molecule FRET trajectories using hidden Markov modeling. *Biophys J*. 2006; 91:1941–1951. [PubMed: 16766620]
33. Scheer H. Biliproteins. *Angew Chem Int Ed*. 1981; 20:241–261.
34. Langer E, Lehner H, Rudiger W, Zickendrahtwendelstadt B. Circular-Dichroism of C-Phycocerythrin - a Conformational Analysis. *Z Naturforsch C*. 1980; 35:367–375.
35. Bischoff M, et al. Excited-state processes in phycocyanobilin studied by femtosecond spectroscopy. *J Phys Chem B*. 2000; 104:1810–1816.
36. Braslavsky SE, Holzwarth AR, Schaffner K. Solution Conformations, Photophysics, and Photochemistry of Bile-Pigments - Bilirubin and Biliverdin Dimethyl Esters and Related Linear Tetrapyrroles. *Angew Chem Int Ed*. 1983; 22:656–674.
37. Su-Ping Z, et al. Generation and identification of the transient intermediates of allophycocyanin by laser photolytic and pulse radiolytic techniques. *Int J Radiat Biol*. 2001; 77:637–642. [PubMed: 11382343]
38. Beladakere NN, et al. Photovoltaic Effects and Charge Transport Studies in Phycobiliproteins. *Mat Res Soc Symp Proc*. 1993; 292:193–198.
39. Katona G, et al. Conformational regulation of charge recombination reactions in a photosynthetic bacterial reaction center. *Nature Struct Biol*. 2005; 12:630–631.
40. Belcher J, Sansone S, Fernandez NF, Haskins WE, Brancalona L. Photoinduced Unfolding of beta-Lactoglobulin Mediated by a Water-Soluble Porphyrin. *J Phys Chem B*. 2009; 113:6020–6030. [PubMed: 19351165]

41. Nesvadba P, Gossauer A. Synthesis of Bile-Pigments. 14 Synthesis of a Bilindionostilbenoparacyclophane as a Model for Stretched Bile Pigment Chromophores of Biliproteins. *J Am Chem Soc.* 1987; 109:6545–6546.
42. Greene BI, Lamola AA, Shank CV. Picosecond Primary Photoprocesses of Bilirubin Bound to Human-Serum Albumin. *Proc Natl Acad Sci USA.* 1981; 78:2008–2012. [PubMed: 6941267]
43. Margineanu A, et al. Visualization of membrane rafts using a perylene monoimide derivative and fluorescence lifetime Imaging. *Biophys J.* 2007; 93:2877–2891. [PubMed: 17573424]
44. Gilson MK, Honig BH. The Dielectric-Constant of a Folded Protein. *Biopolymers.* 1986; 25:2097–2119. [PubMed: 3790703]
45. Kartalov E, Unger M, Quake SR. Polyelectrolyte surface interface for single-molecule fluorescence studies of DNA polymerase. *BioTechniques.* 2003; 34:505–510. [PubMed: 12661156]
46. Ong LJ, Glazer AN. Crosslinking of Allophycocyanin. *Physiol Veg.* 1985; 23:777–787.
47. Mao HB, et al. Effects of glycerol and high temperatures on structure and function of phycobilisomes in *Synechocystis* sp PCC 6803. *FEBS Lett.* 2003; 553:68–72. [PubMed: 14550548]
48. He JA, Hu YZ, Jiang LJ. Photodynamic action of phycobiliproteins: In situ generation of reactive oxygen species. *Biochim et Biophys Acta Bioenerg.* 1997; 1320:165–174.
49. Zander C, et al. Detection and characterization of single molecules in aqueous solution. *Appl Phys B.* 1996; 63:517–523.
50. Pawitan, Y. In *All Likelihood: Statistical Modeling and Inference Using Likelihood*. Clarendon Press; Oxford: 2001. 528

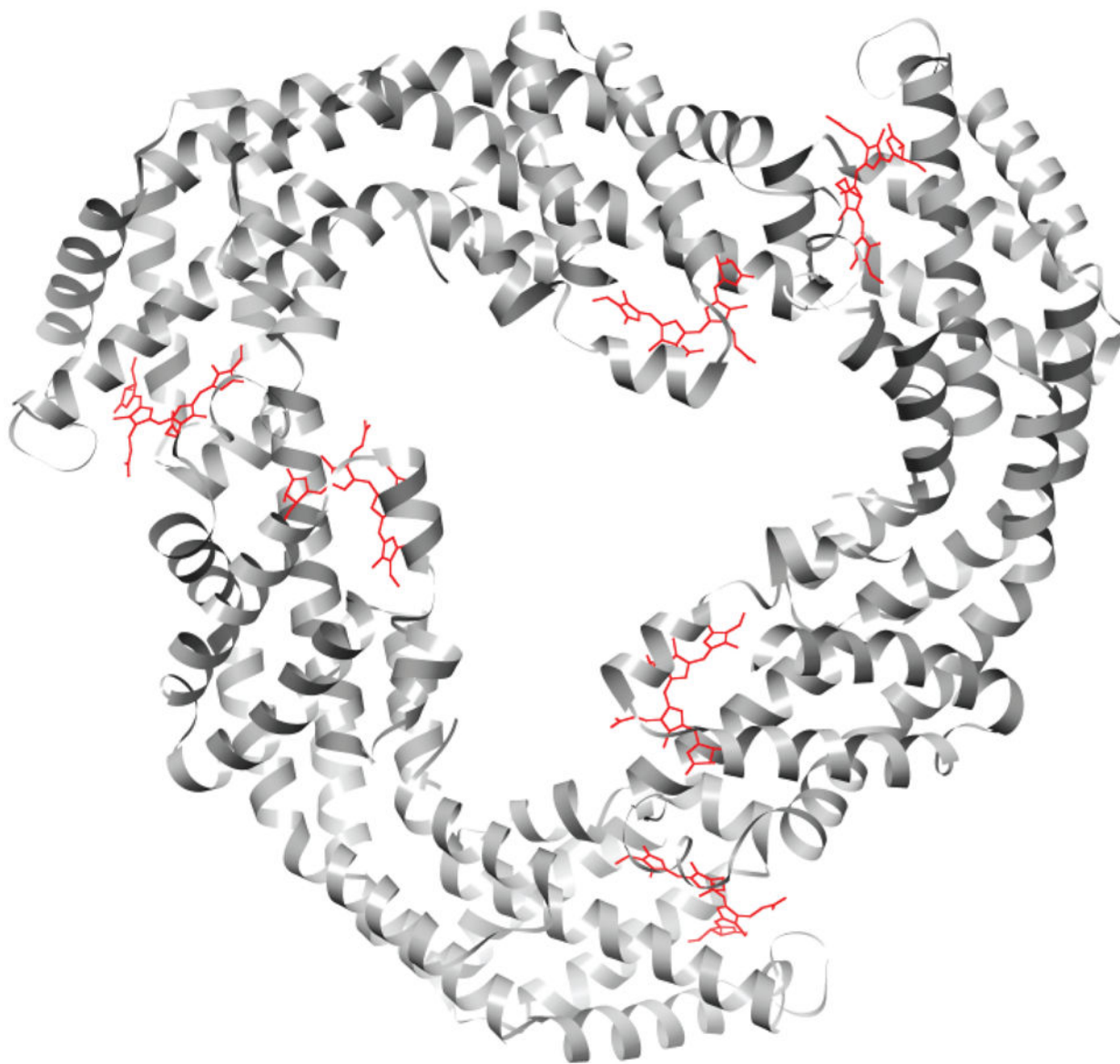


Figure 1. Structure of APC

Each monomer of the APC trimer contains two phycoerythrin (PEB) chromophores (red).

The strongest interaction between pairs of PEB's is at the interface between the subunits.

Produced from PDB structure 1ALL.²²

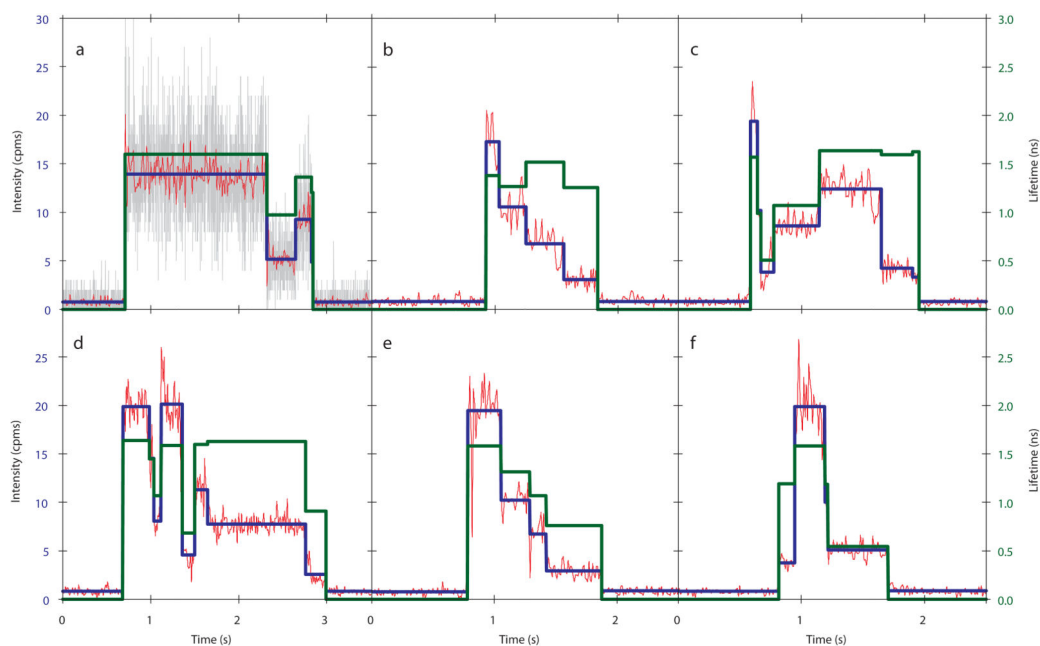


Figure 2. Intensity and lifetime dynamics of single molecules of APC trapped in the ABEL trap (a-f) Traces for six individual trapped APC molecules displaying fluorescence intensity binned at 10 ms (red, left axis), the average intensity from intervals defined by the change-point-finding algorithm (blue, left axis), and lifetimes from those same intervals (green, right axis). Multiple intensity plateaus are easily identifiable. Shifts in intensity and lifetime are sometimes found to be correlated (**a,e,f**), anticorrelated (**b**), or non-correlated (**c,d**). Trace **a** also includes 1 ms binned data (gray).

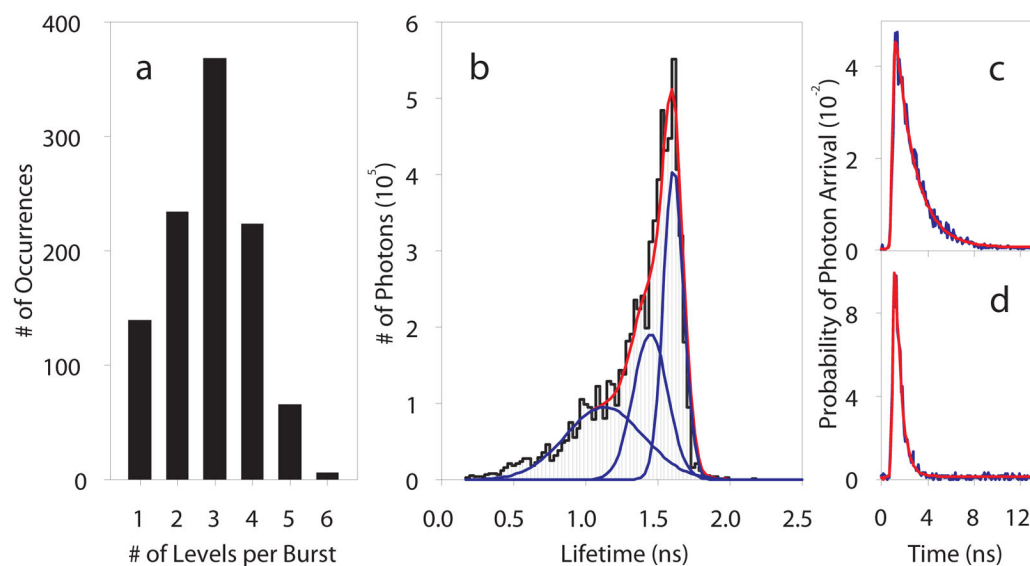


Figure 3. Intensity level and lifetime histograms

a Histogram of the number of APC molecules showing between one and six distinct intensity levels, suggesting at least four observable APC microstates. **b** Histogram of the number of photons collected as a function of fluorescence lifetime with a compound fit (red trace) to three component Gaussians (blue traces). The narrow main peak suggests limited inhomogeneous broadening. **c** An example of a single-molecule fluorescence decay (blue trace) with fit (red trace) yielding $\tau = 1.64$ ns from 6034 photons. **d** Another molecule with $\tau = 0.52$ ns from 1268 photons.

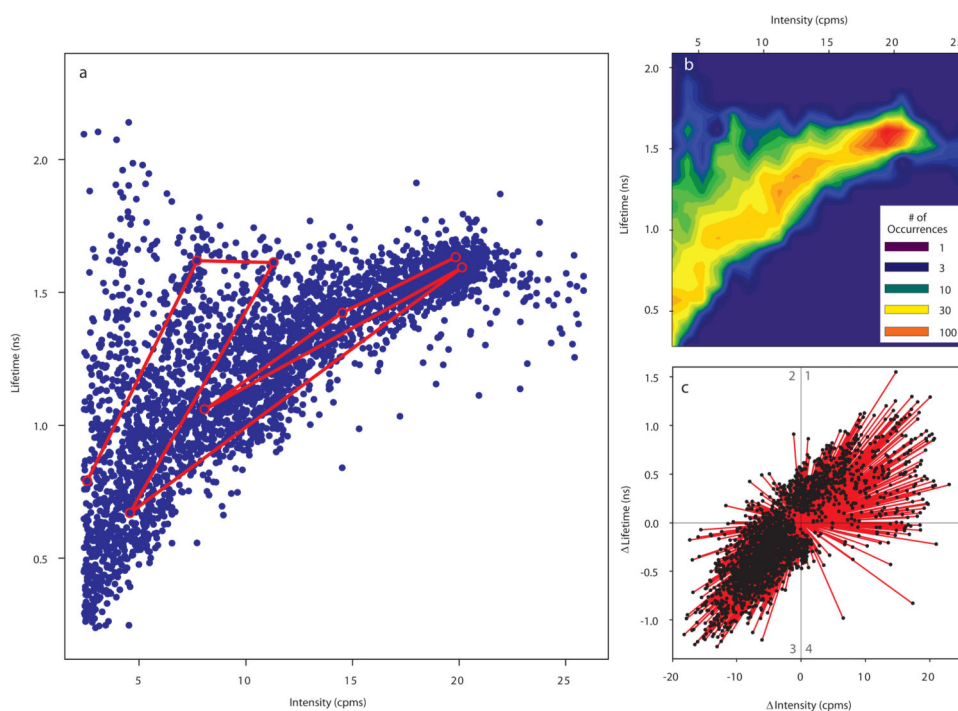


Figure 4. Correlations between fluorescence intensity and lifetime suggest conformational dynamics

a Fluorescence intensity and lifetime for intensity intervals of 1,048 molecules with the intensity-lifetime trajectory of one APC (from Fig. 2d) superimposed in red. Transitions to or from intervals with <200 recorded photons did not yield lifetimes of sufficiently small expected error and were not included in the plot. **b** Contour plot of **a** highlighting the dense grouping at 20 cpms. **c** Individual intensity-lifetime trajectory shifts from 1,048 molecules plotted as vectors beginning at the origin and classified into four quadrants depending on their orientations. Vectors in different quadrants and along different axes indicate discernibly different photophysical processes.

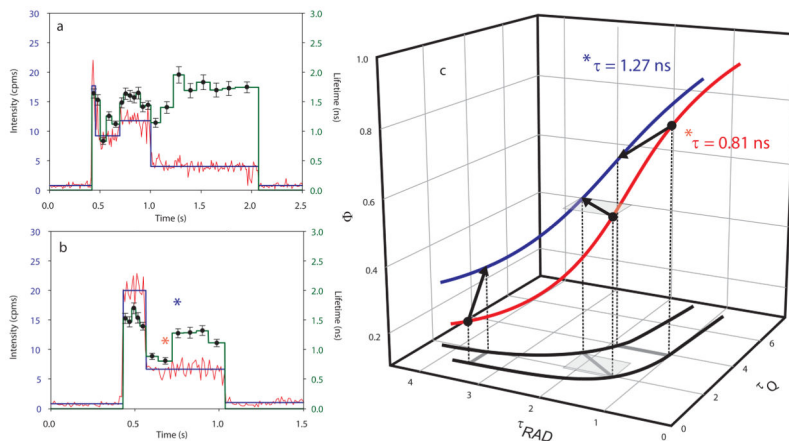


Figure 5. Fluorescence lifetime fluctuations at near constant intensity

a,b Traces for two individual APC molecules displaying fluorescence intensity binned at 10 ms (red, left axis), the average intensity from intervals (blue, left axis), and lifetime measured from consecutive bunches of 500 photons (green, right). Error bars indicate ± 1 standard deviation. **c** Curves of constant observed lifetime, τ , for the starred intervals in **b** from plotting the equation for quantum yield, Φ , in the text. Transitions between the two observed lifetimes are shown with constant τ_{RAD} (left), constant Φ with requisite changing of τ_Q and τ_{RAD} (middle), and constant τ_Q (right). The middle process likely describes the transition between the starred intervals in **b**.

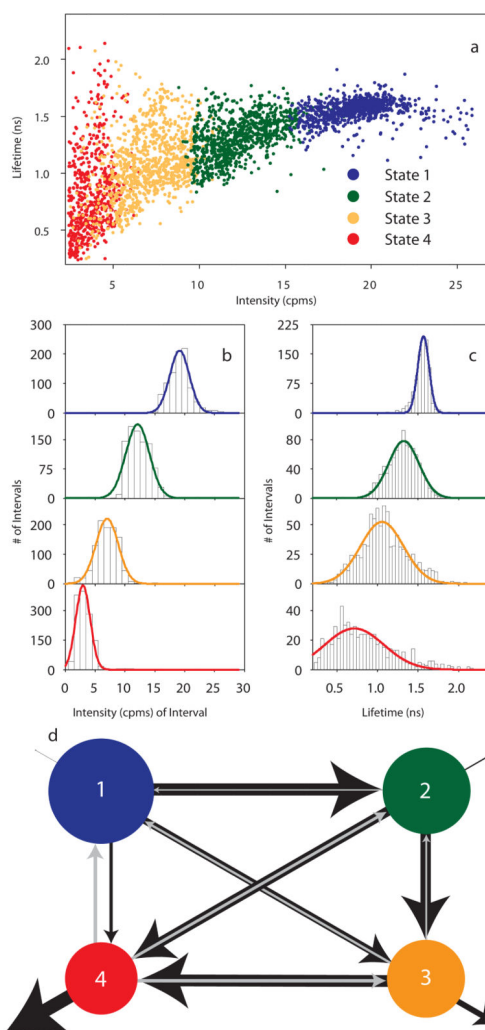


Figure 6. Results from state identification by Time-Order Clustering

a Coloring of data points by state number on the Intensity-Lifetime correlation plot and showing interpenetrating microstates. **b** Histogram of intensity levels of intervals belonging to each state. **c** Histogram of fluorescence lifetimes of intervals belonging to each state with progressively widening distribution. **d** Summary of interstate dynamics calculated from the transition probabilities determined by TOC. Sizes of nodes denote the relative amount of time spent in each state. Black arrows denote transitions to a lower state and gray arrows to a higher state. Arrows to the outside denote irreversible photobleaching/trap loss. The relative size of the arrows is indicative of the relative size of the rate constant, with the largest arrow emerging from state 4 representing 3.1 s^{-1} . Single molecules of APC tend to enter the trap in State 1, then shift to higher numbered states where they are dimmer, show larger distributions of fluorescence lifetime, and are increasingly likely to irreversibly photobleach and/or be lost by the trap.